Indian Journal of Pure & Applied Physics
Vol. 58, January 2020, pp. 50-62

Structural and optical properties of TeO_2- SeO_2-Na_2O glass system

P Satya Gopal Rao[a], Rajesh Siripuram[b] & Suresh Sripada[c*]

[a]Department of Physics, GRIET, Bachupally, Kukatpally, Telangna 500 090, India

[b, c*]Department of Physics, JNTUHCEJ, Nachupally,Telangana 505 501, India

Received 8 August 2018; accepted 2 December 2019

80 TeO_2-(20-x) SeO_2-xNa_2O (where x = 0, 5, 10, 15, 20 mol %) ternary glass system have been successfully prepared by conventional melt-quenching method. The non-crystalline nature of the tested glass samples has been confirmed by X-ray diffraction. The structural transformation in the tested glass samples has been evaluated by measuring density (ρ), molar volume (V_M), oxygen packing density (OPD) and oxygen molar volume (V_0) values. The characteristic temperature of the glass system (glass transition,T_g, crystallization, T_c) decreases with increasing Na_2O content. Raman spectra show that addition of Na_2O to TeO_2 + SeO_2 glass may result in cleavage of Te-O-Te and Se-O-Se linkages and formation of TeO_3^- and SeO_3^- terminal groups in the glass system. FTIR spectra show that the units of TeO_4 units decrease and the units of TeO_3 / TeO_{3+1} increase in the tested glass samples. The cut-off wavelength (λ_C), optical band gap (E_{opt}), refractive index (n), molar refraction (R_M), metallization criterion (M), molar polarizability (α_m), electronic polarizability of oxide ion (α_o^{2-}), optical basicity (Λ), Fermi energy (E_F), dispersion energy (E_d), single oscillator energy (E_0) and Urbach energy (ΔE) have been calculated from optical absorption spectra. The reflectivity of light and extinction coefficient (k) is used to find imaginary part of dielectric constant (ε_i). The optical band gap energy and allowed transitions have been investigated using five methods; indirect, direct, indirect forbidden, direct forbidden and imaginary part of the dielectric constant. The optical band gap values of direct transition are in well agreement with the optical band values of an imaginary part of dielectric constant. The obtained optical band gap values decrease with increasing sodium oxide in the glass samples. Increase in Urbach energy values in the present glass system is due to an increase in the number of defects in the glass structure. The tested glass samples possess higher values of Urbach energy, molar electronic polarizability, and optical basicity. The excitation energy E_0 decreases with the increase of Na_2O content in the glass system.

Keywords: Raman spectra, IR spectra, Tellurite based glasses, Glass matrix, Optical properties

1 Introduction

Tellurite glasses have excellent properties such as good infrared transmissivity (5.5 μm), high devitrification resistance, high refractive index (1.8–2.3), high dielectric constant (10–35), thermal and chemical stability, and show relatively low-phonon energy (600–850 □ω/cm), low glass transition (~300 °C) and melting temperature (below 1000 °C). It's because of these properties; the glasses have potential applications such as non-linear optical devices, electrical behavior in semi-conductivity, electronic switching effects, optical fiber amplifiers[1-10]. Selenite glasses also have tremendous applications such as super-ionic semiconductors, non-linear optical devices, sensors, solar cells, photocells, reflecting windows[11-17]. Adding selenium oxide to tellurite glasses decreases the melting temperature of the glass and changes its optical properties[18,19]. Authors have reported on physical, thermal, structural and optical properties on binary telluride glass system and tellurite ternary glass system using glass formers[5, 9, 20-23]. There are not many studies on conditional glass formers like tellurium and selenium oxides. The formation of glass on two conditional glass formers such as TeO_2 glass and SeO_2 glass is of scientific, technological and practical interest. Adding a small amount of modifier like Na_2O to pure TeO_2-SeO_2 becomes a glass former. This may lead to the formation of new structural units like cleavage of Te-O-Te, Se-O-Se linkage, and formation of TeO_3^-, SeO_3^- terminal groups. The present investigation suggests that increasing Na_2O content acts as a network modifier breaking up the network structure while bringing down the SeO_2 content acting as a network former in the structure with constant TeO_2. The objective of the present work is to understand physical, thermal, structural and optical properties of sodium-selenite-tellurite glasses.

*Corresponding author
(E-mail: sripada_suresh2020@rediffmail.com)

2 Experimental Details

80 TeO_2-(20-x) SeO_2-xNa_2O (x = 0, 5, 10, 15, 20 mol %) ternary system were prepared by conventional melt-quenching method. High purity-grade oxides of TeO_2 (99 %, Aldrich), SeO_2 (99.8%, Aldrich), and Na_2Co_3 (99.0 %, Aldrich) are used for the synthesis of glass samples. These oxides are very much blended in proper extent to shape 5g clusters. The blended extent was grounded in a mortar with a pestle for 30 min to get homogeneity. Each group was liquefied in porcelain crucible with an open lid at 720-750 °C for 30 min in an electric heater to get without bubble free liquid. The dissolve was then extinguished quickly between thick hardened steel plates which were warmed at 200 °C to avoid excess thermal shocks. These glasses are annealed for 4 h at 200 °C to relieve from mechanical strains.

The amorphous nature of the glasses at room temperature was determined using X-Ray diffraction by XRD-BRUKER D8 ADVANCE. DSC analysis of the glass samples was investigated by NETZSCH DSC 204 with a heating rate of 10.0 (K/min) up to 350 °C to determine glass transition (T_g), onset crystallization temperature (T_c). Glasses were grinded to obtain infrared spectra by IR- BRUKER OPTICS TENSOR 27 in the range from 4000 to 600 cm^{-1} at room temperature. Raman spectrometer RAMAN-HORIBA JOBIN YOUN, MODEL- LABRAM 633 nm laser wavelength was used to find out its structural behavior at room temperature. Optical absorption spectraare observed in the wavelength range of 200-1200 nm at room temperature using Varian, Cary 5000 UV-Vis-NMR spectrometer. The composition of the glasses and the corresponding sample codes are listed in Table 1.

3 Results and Discussion

3.1 XRD patterns

The glass system 80 TeO_2-(20-x) SeO_2-xNa_2O prepared under the applied conditions with compositions (where x=5, 10, 15, 20 mol %) are visually transparent and sample where x=0 was opaque. The opaque sample was white in color and other transparent samples were light yellowish in color. The XRD was used to determine the structure, crystalline and non-crystalline of a material. The XRD pattern of tested glass samples are shown in Fig. 1. The X-ray diffraction spectrum of glass samples showed a broad hump indicates that the sample was not a crystal but non-crystalline, i.e., amorphous in nature. The ITSN1 sample is does not form a glass because of a lone pair of electrons, higher oxidation state, and large ionic radius[68]. But it will be prone to crystallization.

Table 1 – Glass sample code and compositions of 80 TeO_2-(20-x) SeO_2-xNa_2O (where x=0, 5, 10, 15, 20 mol %) glass system.

x in mol %	Sample code	Composition (mol %)
x=0	IITSN1	80TeO_2-20SeO_2
x=5	IITSN2	80TeO_2-15SeO_2 - 5Na_2O
x=10	IITSN3	80TeO_2-10SeO_2 - 10Na_2O
x=15	IITSN4	80TeO_2-5SeO_2 - 15Na_2O
x=20	IITSN5	80TeO_2- 20Na_2O

3.2 Physical parameters

Density of the glasses is evaluated with the help of Archimedes' principle using xylene as the immersion liquid[24] using the following relation:

$$\rho = \frac{a*0.86}{(a-b)} \quad \cdot \ldots (1)$$

Where,

a = weight of the sample measured in air,

b = weight of the sample measured in xylene (density of xylene is 0.86 g/cc).

The molar volume of the glass samples are evaluated using the following relation:

$$V_M = \frac{M}{\rho} \quad \ldots (2)$$

Where, M= average molecular weight of the glass, ρ=density.

Oxygen packing density (OPD) of the glass samples are evaluated using the following relation:

$$OPD = \left(\frac{\rho}{M}\right) * number\ of\ oxygen\ atoms\ per\ formula\ unit \quad \ldots (3)$$

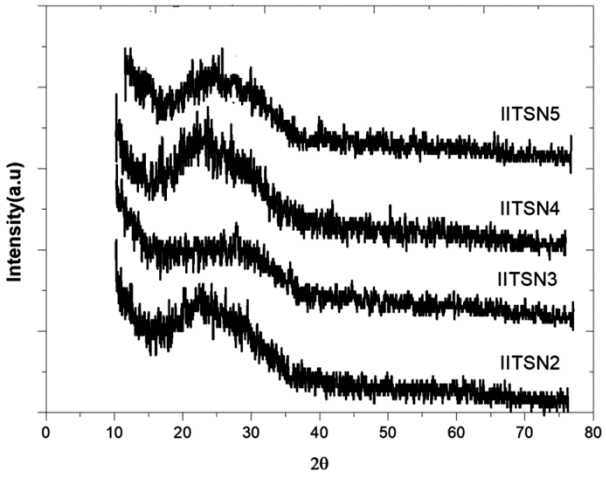

Fig. 1 – X-ray diffraction pattern of 80TeO_2-(20-x) SeO_2-xNa_2O (where x=5, 10, 15, 20 mol %) glass system.

Oxygen molar volume of the glass samples are evaluated using the following relation:

$$V_0 = \left(\frac{\sum x_i M_i}{\rho}\right)\left(\sum \frac{1}{x_i n_i}\right) \quad \ldots (4)$$

Where, x_i = molar fraction of each component 'i', M_i= molecular weight, n_i=number of oxygen atoms in each constituent oxide.

In the present glass system, the density (ρ), V_M, *OPD*, and V_0 values are calculated by increasing Na_2O and decreasing SeO_2 content with constant TeO_2 are listed in the Table 2. The obtained values are plotted and shown in Figs (2 and 3). The measured density of the glasses was found to be in the range of 5.143 to 4.770 g/cc. The V_M values of the present glass system vary from 29.091-31.207 cc/mole. The *OPD* values vary from 67.029 to 57.679 gatom/l and V_0 values vary from 14.918-17.337 cc/mole in the present glass system.

The theoretical density (ρ_{theo}) values were determined using the constituent oxides of appropriate compositions. It is clearly seen from the Fig. 2 that the density (ρ_{expt}) and the molar volume show the opposite behavior. It is observed from the Table 2 there is a minor difference between the theoretical density values (ρ_{theo}) and the measured density values (ρ_{expt}). The minor difference in density values is due to the variation in atomic arrangement between the structure of glass and molecules of the constituent oxides. The density values decreases with increasing Na_2O and decreasing SeO_2 content in the glass system due to a lower molecular weight of Na_2O comparing with TeO_2 and SeO_2 oxides. The increasing molar volume values with increasing Na_2O and decrease in SeO_2 content results in the formation of excess free volume by opening up the glass matrix. From Fig. 3, the oxygen packing density and oxygen molar volume values show the opposite behavior. The oxygen packing density values were found to decrease with increasing Na_2O and decreasing SeO_2 content. This behavior is due to the decrease in the number of oxygen atoms per unit composition and it results in fewer linkages in the glass matrix. The oxygen molar volume values were found to increase with increasing Na_2O and decreasing SeO_2 content. This behavior could be explained by the substitution of SeO_2 with Na_2O which leads to looseness of packing of the glass network with degradation of Te–O–Se and Se–O–Se linkages. From the above results, it is concluded that formation of less dense structure and less tightly packing results in degradation of structural units and formation of non-bridging oxygen sites in the glass matrix. The similar behaviors were observed by Miray Celikbilek *et al*.[24] in TeO_2- WO_3-Na_2O and Kutlu B *et al*.[25] in the TeO_2-Na_2O glass system.

Table 2 – Physical and thermal properties of 80 TeO_2-(20-x) SeO_2-xNa_2O (x=5, 10, 15, 20 mol %) glass system.

Property	x=5	x=10	x=15	x=20
ρ_{expt} (g/cc)	5.143	4.968	4.964	4.770
ρ_{theo} (g/cc)	4.716	4.574	4.438	4.862
V_M(cc/mole)	29.091	30.062	30.036	31.207
OPD(g.atom/l)	67.029	63.202	61.592	57.679
V_0(cc/mole)	14.918	15.821	16.236	17.337
$T_g{}^oC$	294	275	249	247
$T_c{}^oC$	329	309	280	275
$\Delta T(^oC)$	35	34	31	28

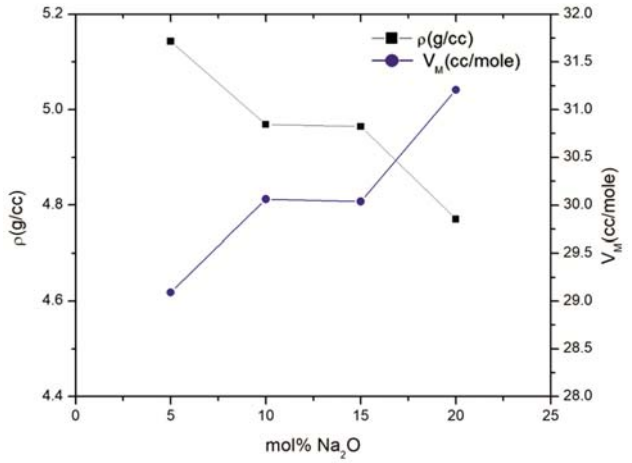

Fig. 2 – Variation of density, ρ, molar volume and V_M values with increasing Na_2O content.

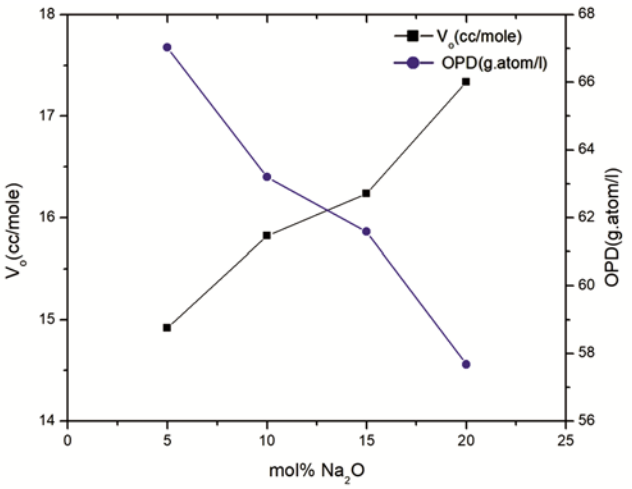

Fig. 3 – Variation of oxygen molar volume, V_O, oxygen packing density and *OPD* values with increasing Na_2O content.

3.3 Thermal analysis

Thermal behavior of 80TeO_2–(20-x) SeO_2–xNa_2O with x=5, 10, 20, 30 mol % glasses are determined by performing DSC analysis and obtained thermo grams are shown in Fig. 4. DSC analysis of the glass samples showed an exothermic peak representing phase transformation and crystallization of different phases. The obtained values of glass transition temperature (T_g) and onset crystallization temperature (T_c) are listed in Table 2. All glass samples showed the broad exothermic change between 294 °C and 247 °C corresponds to the glass transition temperature (T_g). From Table 2, it has been observed that T_g values decrease with decreasing SeO_2 mol % and increasing Na_2O mol %. The decrease in glass transition temperature is due to weaker Se-O bonds whose binding energy is less than Te-O bond binding energy[26]. The onset crystallization temperature (T_c) values from the thermo grams are observed between 329 °C and 275 °C. As the concentration Na_2O mol % increases (SeO_2 mol % decreases), the onset crystallization temperature decreases. The decrease in onset crystallization temperature with decreasing SeO_2 mol % and increasing Na_2O mol % is due to the decrease in the number of bonds per unit volume[8, 24], which results in the less tightly packing in the glass matrix. These results suggest that Se_2O act as conditional network former and Na_2O acts as a network modifier by breaking up the glass network structure. The glass stability, $\Delta T=T_c-T_g$ values are calculated and listed in Table 2.

3.4 Raman spectra

The Raman spectra of 80 TeO_2-(20-x) SeO_2-xNa_2O (where, x=5, 10, 15, 20 mol %) glasses are recorded and shown in Fig. 5. In the present investigation, the absorption bands are observed in the wave number range of 325-332 cm^{-1}, 450-476 cm^{-1}, 663-676 cm^{-1}, 700-739 cm^{-1} and 753-786 $cm^{-1}$and are presented in Table 3. Their corresponding peak assignments are listed in Table 4. The band 325-332 cm^{-1} is assigned to vibrations of TeO_3 (tp) overlapping with Se-O-Se and /or Te-O-Se vibrations[27]. The band around 450-476 cm^{-1} is attributed to symmetric bending vibration of TeO_4 (tbp) while symmetric stretching vibration of Te–$_{eq}O_{ax}$–Te linkages are formed by vertex sharing TeO_4 (tbp) and bending vibrations of Te-O-Te or Te-O-Se linkages[28-37]. The high-intensity Raman band 663-676 cm^{-1} is assigned to a symmetrical stretch of Te-O bonds in TeO_4 units combined vibrations of asymmetric stretching of Te–$_{eq}O_{ax}$–Te bonds and

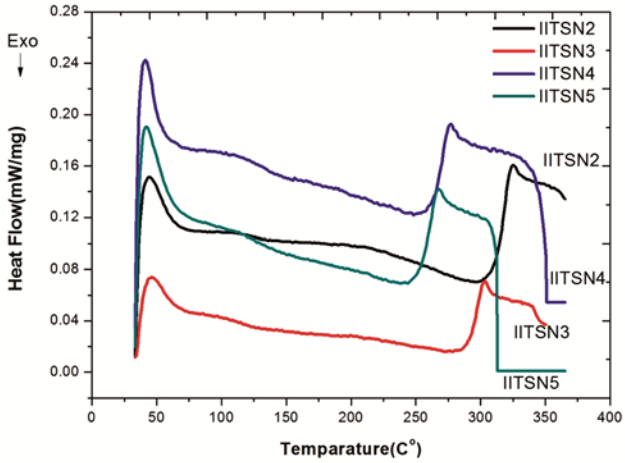

Fig. 4 – DSC curves of 80 TeO_2-(20-x) SeO_2-xNa_2O (x=5, 10, 15, 20 mol %) glass system.

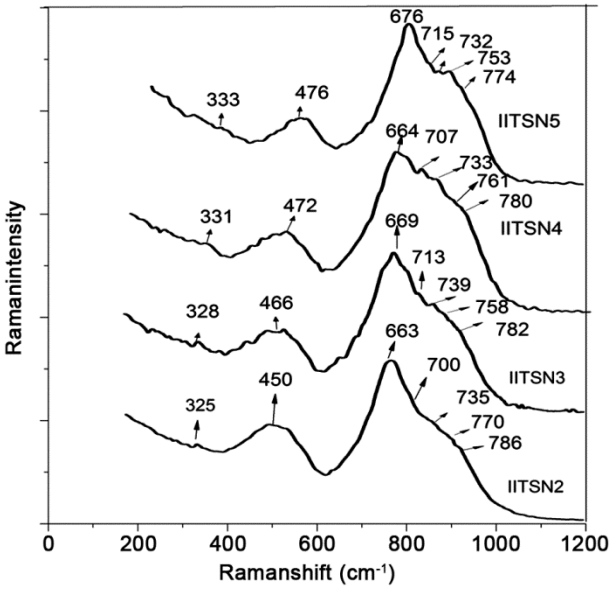

Fig. 5 – Raman spectra of 80 TeO_2-(20-x) SeO_2-xNa_2O (where x=5, 10, 15, 20 mol %) glass system.

Table 3 – Raman peak frequencies of 80 TeO_2-(20-x) SeO_2-xNa_2O (where x=5, 10, 15, 20 mol %) glass system.

Sample code	Peak positions (cm^{-1})						
IITSN2	325	450	663	700	735	770	786
IITSN3	331	466	669	713	739	758	782
IITSN4	332	472	664	707	733	761	780
IITSN5	328	476	676	715	732	753	774

stretching mode of the TeO_3 trigonal pyramid (tp) units[38-40]. The Raman band around 700-739 cm^{-1} is assigned to the vibration of TeO_4 groups[41, 42]. The low intensity Raman band 753-786 cm^{-1} is assigned to stretching vibration of TeO_3 polyhedra or TeO_{3+1} (tp) units[43].

Table 4 – Peak assignments of raman bands of 80 TeO_2-(20-x) SeO_2-xNa_2O (where, x=5, 10, 15, 20 mol %) glass system.

Peak frequencies (cm^{-1})	Peak assignments
325-332	vibrations of TeO_3 tp overlapped with Se-O-Se and/or Te-O-Se
450-476	Te–$_{eq}O_{ax}$–Te linkages and bending vibrations of Te-O-Te or Te-O-Se linkages
663-676	symmetrical stretch of Te-O bonds in a TeO_4 units and stretching mode of the TeO_3 trigonal pyramid (tp) units
700-739	the vibration of TeO_4 groups
753-786	stretching vibrations of TeO_{3+1}polyhedra or TeO_3 trigonal pyramid (tp) units.

It is observed from the Raman spectrum that each spectrum showed broad peaks and shoulders reveals the disorder nature of the glass system. It is noticed that the intensity of Raman bands in the range of 450-476 cm^{-1} decreases and peaks move towards higher wave number from 450 cm^{-1} to 472 cm^{-1} due to the breakage of Te-O-Te or Te-O-Se linkages as Na_2O mol % increases. This implies that the modifier reduces the hardness of relevant bonds and the rigidity of the glassy network. The strong peak in the region 663-676 cm^{-1} is due to the formation of stretching vibrations of TeO_4 trigonal bipyramids (tbps) units and bending mode of Te-O-Te or O-Te-O linkages. The peaks are in the region 774-786 cm^{-1} is due to the formation of TeO_4 trigonal bipyramids (tbps) to TeO_3 trigonal pyramids (tps) via intermediate type TeO_{3+1} polyhedra or TeO_3 trigonal pyramid units. The weak Raman band at 786 cm^{-1} for IITSN2 sample is shifting to lower wavelength side 7774 cm^{-1}(786 cm^{-1} →782 cm^{-1} →780 cm^{-1} →774cm^{-1}) as Na_2O mol % increases in the present glass system. It is also observed in the Fig. 5 for IITSN2 glass sample the weak shoulder is broadening as Na_2O mol % increases from 5 to 20 mol % in the glass samples. This behavior could be related to vibration modes arising from glass former and glass modifier, which results in the number of TeO_4 structural unit's decrease and that of the TeO_3 structural unit increase with increasing Na_2O content in the glass samples. This results in increase of non-bridging oxygens concentration (NBOs) in the glass matrix. In the present glass system it can be concluded that with the increase in Na_2O mol % (SeO_2 mol % decrease) the coordination number of TeO_2 leads to a gradual reduction of the tellurium coordination number from TeO_4(tbps) to TeO_3(tps) with the increase in number of non-bridging oxygens. Such a change in coordination number is associated with the formation of more number of non-bridging oxygens than bridging oxygens (BOs) in the glass matrix.

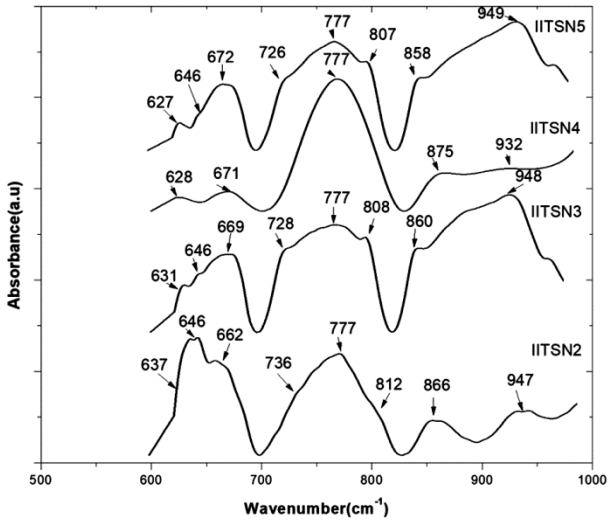

Fig. 6 – IR spectra of 80 TeO_2-(20-x) SeO_2-xNa_2O (where x=5, 10, 15, 20 mol %) glass system.

3.5 IR spectra

The IR spectra of 80 TeO_2-(20-x) SeO_2-xNa_2O (where x=5, 10, 15, 20 mol %) glasses are recorded and shown in Fig. 6 (as absorbance units versus wave number). In the present investigation, the absorption bands are observed in the range of 627-669 cm^{-1}, 726-777cm^{-1}, 807-875 cm^{-1}, and 932-949 cm^{-1} are presented in Table 5. Their corresponding peak assignments are listed in Table 6. The absorption bands located around 627-669 cm^{-1} are assigned to asymmetric vibrations of TeO_4 (tbps) and vibration of symmetrical TeO_3 groups[44-46]. The band located in the range of 726-777cm^{-1} is assigned to stretching mode of TeO_3 (tps) with non-bridging oxygens[24, 25, 47, 48]. The band located around 807-812 cm^{-1} is assigned to Te–O bending vibrations[49] in TeO_3. The absorption band located in the range of 858−880 cm^{-1} is ascribed to the vibration mode of the Se−O−Se bond of SeO_3^{2-}ions[50]. The bands located around 932-950 $cm^{-1}$is assigned to isolated pyramidal SeO_3 groups[45, 46, 51].

Two modes of vibrations regions are noticed in the case if tellurium glass structure The first band occurs at 600-646 cm^{-1} for TeO_4 (tbp) and second band occurs at 660-700 for TeO_3 (tp)[44].The absorption region around 627-646 cm^{-1} in the present study may be assigned to asymmetric vibrations of TeO_4 (tbp) structural units. However, the absorption region around 662-672 cm^{-1} is assigned to vibration of symmetrical TeO_3 groups. In the present study, it is

Table 5 – Infrared absorption bands of $80TeO_2$-(20-x) SeO_2-xNa_2O (where x=5, 10, 15, 20 mol %) glass system.

Sample code	Peak positions (cm^{-1})								
IITSN2	637	646	662	736	777	812	866	947	947
IITSN3	631	646	669	728	777	808	860	948	948
IITSN4	628	----	671	----	777	---	875	932	932
IITSN5	627	646	672	726	777	807	858	949	949

Table 6 – Peak assignments of IR bands of $80TeO_2$-(20-x) SeO_2-xNa_2O (where x=5, 10, 15, 20 mol %) glass system.

Peak frequencies (cm^{-1})	Peak assignments
627-646	asymmetric vibrations of TeO_4(tbp)
662-672	the symmetrical vibration of TeO_3 groups
726-777	stretching mode of TeO_3(tp) with(NBO)
807-812	Te–O bending vibrations in TeO_3 groups
858-880	vibration mode of the Se−O−Se bond of SeO_3^{2-}ions
932-950	isolated and pyramidal SeO_3 groups

assumed that there is an existence of both TeO_4 and TeO_3 structural units in the glass matrix. The shoulder at 662 cm^{-1} for the glass sample IITSN2 at x=5 mol % turn out to be a broad peak as Na_2O mol % increases from x=5 to 20 mol % in the glass samples, which results in the transformation of TeO_4 structural units into TeO_3 structural units. The weak shoulders at 736 cm^{-1} for the glass sample IITSN2 at x=5 mol % is broadly enhanced at 728 cm^{-1} for the glass sample IITSN3 at x=10 mol % and 726 cm^{-1} for the glass sample IITSN5 at x=20 mol %. The decrease in absorption region 736-726 cm^{-1}(736 cm^{-1}→728 cm^{-1}→726 cm^{-1}) for all the tested glass samples could be related to the Te–O stretching vibrations of TeO_4 trigonal bipyramid (tbp) units decrease, and the peaks related to the TeO_{3+1} ployhedra or TeO_3 trigonal pyramids (tps) increased due to the formation of non-bridging oxygens (NBOs) in the glass sample. Dimitriev *et al.*[51] reported that a weak band at 780cm^{-1} in a TeO_2-SeO_2 glass system is attributed to TeO_3 trigonal pyramids (tps) with NBOs or TeO_{3+1}units. Hager *et al.*[42] reported that the addition of Na_2O to tellurite glasses may cause the vibration of TeO_3 groups around the absorption region 745–790 cm^{-1}. The high-intensity band observed at 777 cm^{-1} did not change despite changing the SeO_2 and Na_2O mol % for all the glass samples. In the present study, the absorption band around 777 cm^{-1} attributed to symmetric and anti-symmetric stretching vibration of the TeO_3 trigonal pyramid (tp) with NBO or TeO_{3+1} unit[42]. The weak shoulders at 812 cm^{-1} for the glass sample IITSN2 is turn out to peak at 808 cm^{-1} for the glass sample IITSN3 at x=10 mol % and 807 cm^{-1} for the glass sample IITSN5 at x=20 mol %. The decrease in absorption region 812-807 cm^{-1}(812 cm^{-1}→808 cm^{-1} →807 cm^{-1}) for all the glass samples could be related to Te–O bending vibrations in TeO_3 groups, which results in increasing TeO_3 units in the glass matrix. By considering above results it is concluded that the structural investigation of TeO_2-SeO_2-Na_2O glasses results in the formation of non-bridging oxygens (NBOs) in the form TeO_3 and TeO_{3+1} units as Na_2O mol % increase and SeO_2mol % decrease in the glass sample. The formation of non-bridging oxygens in the present glass system is in the form of TeO_{3+1}, TeO_3 unit's results in looseness of packing in the glass structure.

3.6 Optical properties

The investigation of the principal absorption edge in the UV spectra is a valuable technique for the examination of optical changes and electronic band structure in both crystalline and amorphous materials. The analysis of optical absorption spectra (Fig. 7) shows that the principal absorption edges are not sharply defined for all the glass samples. It indicates the glassy nature is observed in the glass samples[23]. A distinct cut-off was observed in all the glass samples. The cut-off wavelengths (λ_C) are noticed for different tested glass samples and are listed in Table 3. The cut-off wavelengths (λ_C) blue shifted due to increase in the rigidity of the glass system with increase of Na_2O mol % in the glass samples. The decrease in cut-off wavelength results, the conversion of structural units from TeO_4 to TeO_3 in the glass matrix[22].

The shape of the fundamental absorption edge in the exponential tail, i.e., Urbach region, provide information on low crystalline, poor crystalline, disordered and amorphous materials because these materials have localized states which are extended in the band gap. In the low photon energy range, the spectral dependence of the absorption coefficient and photon energy is known as Urbach empirical rule.

The absorption coefficient $\alpha(v)$ at a particular temperature was calculated using empirical relation known as Urbach rule[52] given by:

$$\alpha(\nu) = \alpha_0 exp\left[\frac{h\nu}{\Delta E}\right]$$

Taking the logarithm on both sides of the above equation, we get a straight line equation as:

$$ln\,\alpha(\nu) = ln\,\alpha_0 + \left[\frac{h\nu}{\Delta E}\right] \quad \ldots (5)$$

Where, $h\nu$=photon energy, α_o=constant, ΔE=Urbach energy.

Therefore, the ΔE can be determined from the slope of the straight line of plotting *ln (α) vs hν*.

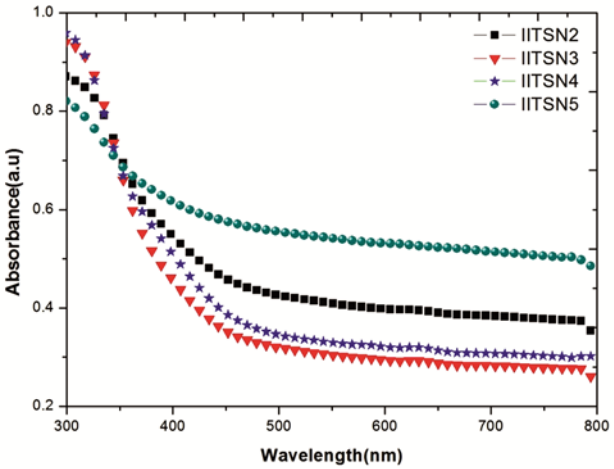

Fig. 7 – Optical absorption spectra of 80 TeO_2-(20-x) SeO_2-xNa_2O (where x=5, 10, 15, 20 mol %).

The absorption coefficient of each spectra are evaluated by the relation:

$$\alpha(\nu) = \frac{2.303A}{t} \quad \ldots (6)$$

Where, *t*=Thickness of the sample.

A=absorbance coefficient for the corresponding thickness of the tested glass sample.

The optical absorption at the fundamental edge is given by the Tauc's[53] equation

$$(\alpha h\nu)^{1/n} = const\left[h\nu - E_{opt}\right] \quad \ldots (7)$$

Where, E_{opt}=optical band gap, $h\nu$=photon energy, *const*=bond tailing parameter.

The exponent *n=1/2, 2, 3/2 and 3* determines the type of electronic transition of direct allowed, indirect allowed, direct forbidden and indirect forbidden band gap, respectively. By plotting $(\alpha h\nu)^{1/n}$ *vs* $h\nu$, one can determine optical band gap for all electronic transitions. E_{opt} values were determined by extrapolating the linear of $(\alpha h\nu)^{1/n}$ *vs* $h\nu$ curve at $(\alpha h\nu)^{1/n}=0$ of the samples are shown in the Fig. 8 (a), (b), (c) and (d). The obtained E_{opt} values for all electronic transitions '*n*' for the tested glass samples

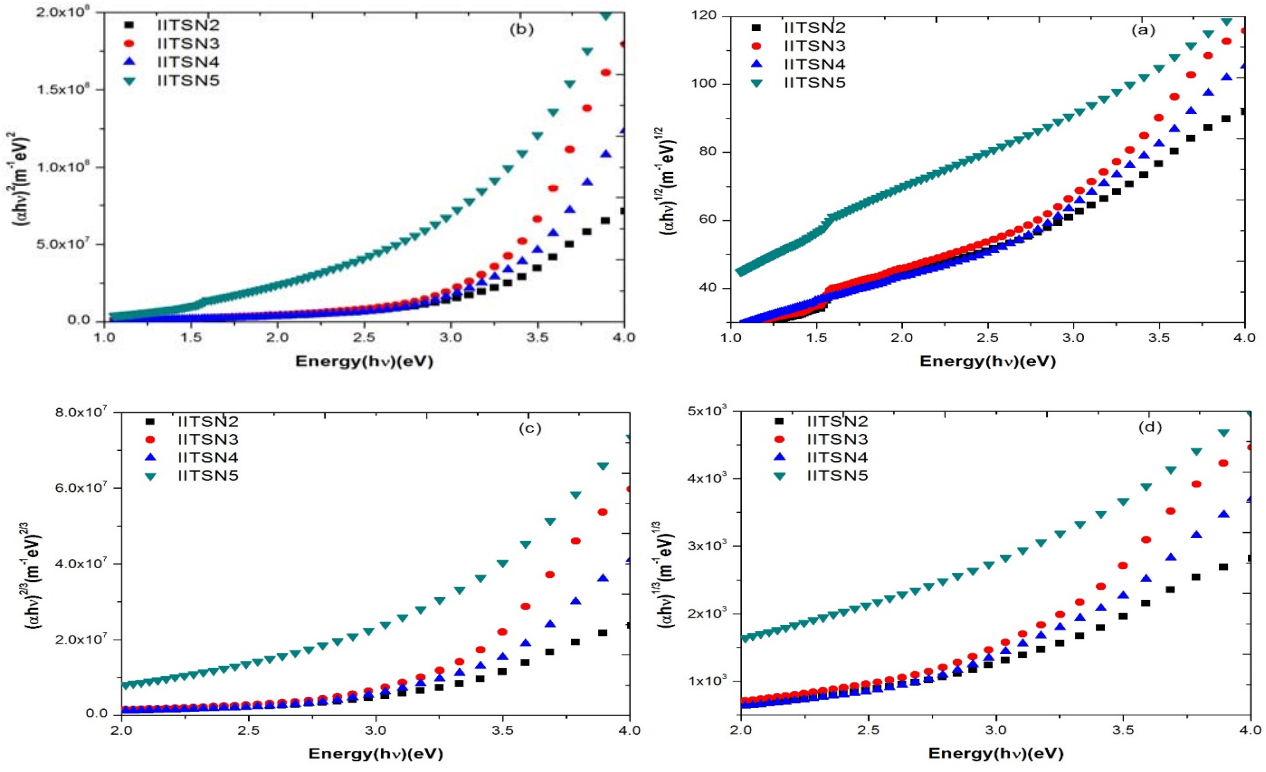

Fig. 8 – The relation between $(\alpha h\nu)^{1/n}$ against photon energy $h\nu$ where *n=1/2, 2, 3/2 and 3* for 80 TeO_2-(20-x) SeO_2-xNa_2O (where x=5, 10, 15, 20 mol %) glass system.

are listed in Table 7. It is clearly noticed from the Table 7 for each exponent '*n*' the E_{opt} values decrease with the increase of Na_2O mol % in the tested glass samples. The obtained values of the optical band gap are varying according to the selected value of each exponent 'n'. From the exponent *n=1/2, 2, 3/2 and 3* one cannot determine exactly which value of exponent '*n*' is better to be selected. Therefore, by using absorption measurements alone one cannot decide which optical band gap values are fitted for the exponent 'n' in glass samples. Hence, the Eq. (7) may be used only for the determination of the type of conduction mechanism[22] in glass materials. To find more accurate optical band gap values Gosain DP *et al.*[54] and L Escobar-Alarcon *et al.*[55] proposed a theory of reflectivity of light. The refractive index (n) and extinction coefficient (k) values can be determined from the theory of reflectivity of light. According to the theory the reflectance of light[22, 54, 55], the reflectivity(R) and extinction coefficient (k) are evaluated by the relation

$$R = \frac{[(n-1)^2 + k^2]}{[(n+1)^2 + k^2]}$$

Or $R = 1 - Texp\left(\frac{t\alpha(\nu)}{2.303}\right)$ … (8)

and

$$k = \frac{\alpha(\nu)\lambda}{4\pi} \quad \cdots (9)$$

Where, λ=wavelength of the incident photon, k=extinction coefficient of the imaginary part of the complex index refraction which relates to light absorption.

The extinction coefficient is utilized to quantify the part of loss of light by scattering and absorption per unit distance of the glass medium. The estimations of the refractive index can choose with respect to reflectivity by using the relation:

$$n^2 = \frac{\left(1+R^{1/2}\right)}{\left(1-R^{1/2}\right)} \quad \cdots (10)$$

Where, R=reflectivity of the sample in the transparent region of glass studied.

Figure 9 and 10 shows the extinction coefficient and refractive index as a function of wavelength for the glass system, respectively. It is clear from Fig. 9

Table 7 – Optical properties of 80 TeO_2-(20-x) SeO_2-xNa_2O (x=5, 10, 15, 20 mol %) glass system.

Property	x=5	x=10	x=15	x=20
λ_C(nm)	477	470	468	452
n=1/2	3.121	3.113	3.105	2.992
n=2	2.489	2.416	2.287	2.047
n=3/2	3.121	3.097	3.113	2.440
n=3	2.519	2.454	2.214	1.676
E_{opt} *from* ε_i	3.176	3.113	3.144	3.000
n	2.365	2.367	2.369	2.399
R_M	17.599	18.201	18.200	19.135
$M(E_{opt})$	0.395	0.394	0.394	0.386
$\alpha_m x10^{-24}$ cm^3	6.879	7.218	7.217	7.588
$\alpha_o^{2-}(E_{opt})Å^3$	2.911	3.106	3.182	3.469
$\Lambda(E_{opt})$	1.096	1.132	1.145	1.188
E_F(eV)	1.379	1.238	1.766	1.770
E_d(eV)	14.002	9.328	10.667	27.277
E_0(eV)	3.570	3.152	3.232	5.237
ΔE(eV)	1.949	1.264	1.355	4.129

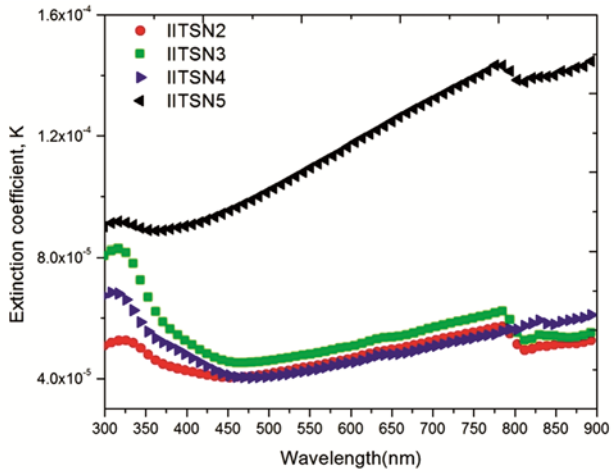

Fig. 9 – The extinction coefficient '*k*' as a function of wavelength for 80 TeO_2-(20-x) SeO_2-xNa_2O (where x=5, 10, 15, 20 mol %) glass system.

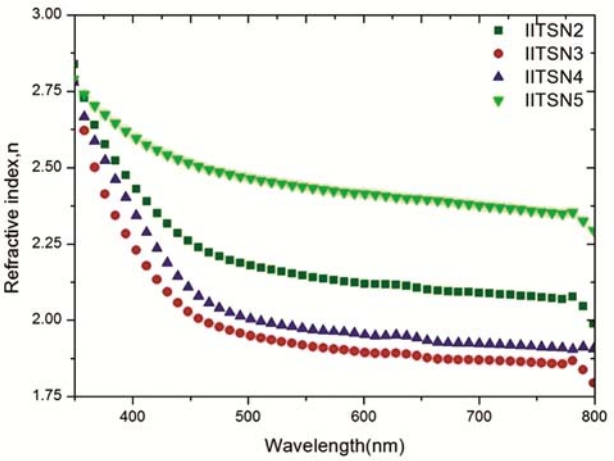

Fig. 10 – The refractive index '*n*' as a function of wavelength for 80 TeO_2-(20-x) SeO_2-xNa_2O (where x=5, 10, 15, 20 mol %) glass system.

that the extinction coefficient found to be decreasing with increasing wavelength (low wavelength region) of the incident photon. It is noticed form the Fig. 10 the decrease in the refractive index indicates that the normal dispersion behavior is observed in the glass samples. The decrease in the extinction coefficient with an increase in wavelength (low wavelength region) results in the fraction of light lost due to scattering and decrease in absorbance.

The complex dielectric study is one of the basic natural properties of the material which contains real and imaginary part. The real part shows the amount of speed of light which slow down in the material. The imaginary part shows the amount of dielectric material that absorbs energy from an electric field because of dipole movement.

The complex dielectric constant is one of the fundamental intrinsic properties of the material. It contains real and imaginary part. The real part shows how much it will slow down the speed of light in the material. The imaginary part shows how much a dielectric material absorbs energy from an electric field due to dipole motion. The extinction coefficient is the imaginary part of the complex index refraction and also relates to light absorption. The ratio of the imaginary and real part of dielectric constant provides information about the loss factor. Real and imaginary parts of the dielectric constant (ε_r, ε_i) are related to the '*n*' and '*k*' values, using the formula:

$$\varepsilon_r = n^2\text{-}k^2 \quad \cdots (11)$$

$$\varepsilon_i = 2nk \quad \cdots (12)$$

Figure 11 shows the variation of ε_r *vs hv* energy for the present glass system. It can be seen clearly from the Fig.11 that the real part of the dielectric constant shows an exponential steady increase with an increase in photon energy.

Figure 12 shows the variation of the ε_i *vs hv* for the present glass system. The imaginary part of the dielectric constant is related to the extinction coefficient and also light absorption. The values of the E_{opt} can be determined by extrapolating in the linear region of the imaginary dielectric constant (ε_i) versus energy curve at $\varepsilon_i = 0$ are listed in Table 7.

By comparing the E_{opt} values obtained from absorption spectra and the values estimated form the imaginary part of the dielectric constant (ε_i), one can find the best fitting exponent for electronic transition is $n=1/2$. Therefore, the E_{opt} values obtained from absorption spectra and imaginary part of the dielectric

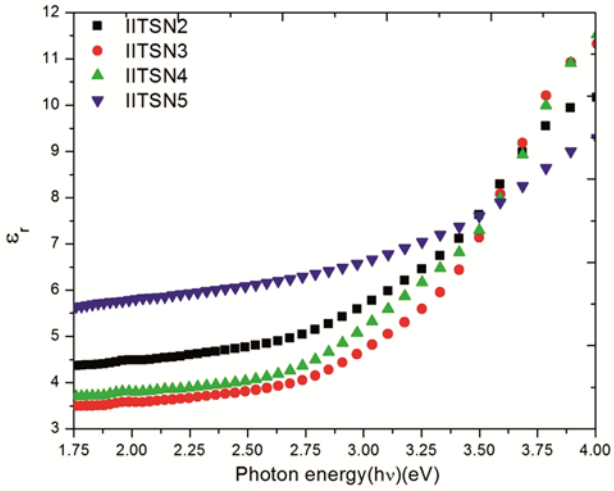

Fig. 11 – The real part of the dielectric constant (ε_r) as a function of photon energy for 80 TeO_2 (20-x) SeO_2-xNa_2O (where x=5, 10, 15, 20 mol %) glass system.

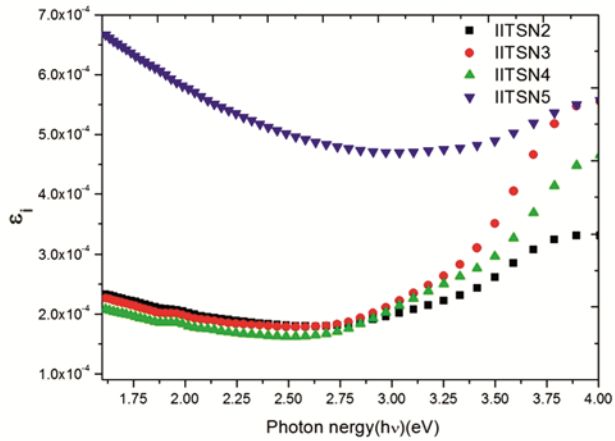

Fig. 12 – The imaginary part of the dielectric constant (ε_i) as a function of photon energy for 80 TeO_2-(20-x) SeO_2-xNa_2O (where x=5, 10, 15, 20 mol %) glass system.

constant measurements are in good agreement for the exponent $n=1/2$. Thus, the direct band gap is present in the tested glass samples.

In the tested glass samples, the direct band gap decreases from 3.121 to 2.992 eV as Na_2O mol % increases. The decrease in E_{opt} values may be associated with the structural change which has been occurred in the glass samples as Na_2O content increases. When Na_2O mol % increases the glass structure becomes a less ordered state, which causes breaking up of the regular structure of tellurite and selenite, leading to a decrease in optical band gap in the present glass system. This decrease is due to an increase in the disorder and more extension of the localized states within the gap. The decrease in the band gap energy also suggests that non-bridging

oxygens (NBOs) concentration increases as Na_2O content increases in the glass samples. Similar behavior is observed by Halimah *et al.*[21] in the glass system (TeO_2-B_2O_3-Ag_2O).

The refractive index in terms of the optical band gap (E_{opt}) of the tested glass samples is calculated by using the equation[59] is:

$$\frac{n^2-1}{n^2+2} = 1 - \sqrt{\frac{E_{opt}}{20}} \quad \ldots (13)$$

It is clearly seen from the Fig. 13 that the refractive index increases from 2.365 to 2.399 due to increase in NBO's as Na_2O mol % increases in the glass samples.The obtained values are higher[56,57] than those for TeO_2–ZnO–Nb_2O_5–Gd_2O_3, $70TeO_2$–$25WO_3$–$5La_2O_3$–Gd_2O_3 glass system. Consequently, there is a direct proportional relationship between polarization and the refractive index could be achieved[58] due to high polarization of the host material[56] TeO_2.

The molar refraction (R_M in cm^3) is calculated by using the equation[59] is:

$$R_M = \left(\frac{n^2-1}{n^2+2}\right) V_M \quad \ldots (14)$$

Where, 'V_M' is the molar volume and 'n' is the refractive index of the glass and the term $\left(\frac{n^2-1}{n^2+2}\right)$ represents reflection loss. The molar refraction values increases from 17.599-19.135 as Na_2O content increase in the glass samples. These values are listed in Table 7.

The theory of metallization criterion $M(E_{opt})$ proposed by Herzfeld[60] to predict whether the glasses are metallic or non-metallic. The metallization criterion is calculated by using the equation[59, 60] is:

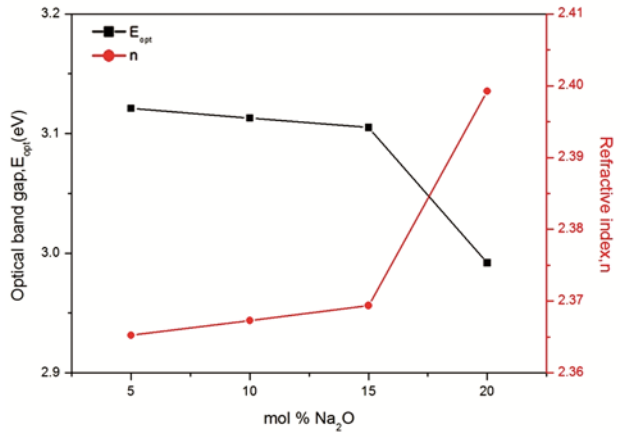

Fig. 13 – The refractive index and optical band gap for 80 TeO_2-(20-x) SeO_2-xNa_2O (where x=5, 10, 15, 20 mol %) glass system.

$$M = 1 - \frac{R_M}{V_M} \quad \ldots (15)$$

The calculated values of 'M' are listed in Table 7. The metallization criterion for the tested glass sample lies in the range of 0.386-0.395. The smaller metallization values for all the glass samples indicates that the width of both conduction band and the valence band become large, which results in the decrease in the optical band gap energy values[56]. If $R_M/V_M > 1$ then the glass exhibits metallic nature and if $R_M/V_M < 1$ then the glass is treated as a non-metallic or insulating nature. From this metallization criterion theory, the present glass system is non-metallic or insulating in nature.

According to the Clausius-Mossotti equation, the molar polarizability (α_m) is proportional to the molar refraction (R_M)[61] of the material is given by the relation:

$$\alpha_m = \left(\frac{3}{4\pi N_A}\right) R_M \quad \ldots (16)$$

Where,'N_A' is Avogadro's number. The calculated values are listed in Table 7. It is observed from the Table 7 the increase in refractive index and molar refraction accompanies the increase in molar polarizability.

The oxide ion polarizability[62, 63] (α_o^{2-}) is based on the optical band gap energy, E_{opt} is evaluated by the relation:

$$\alpha_o^{2-} = \left[\frac{V_M}{2.52}\left(1 - \sqrt{\frac{E_{opt}}{20}}\right) - \sum_i p\alpha_i\right] q^{-1} \quad \ldots (17)$$

where, 'E_{opt}' optical band gap, 'V_M' is molar volume, 'α_i' is polarizability of the molar cations, 'p' and 'q' denote the number of cations and oxide ions respectively in the chemical oxide C_pO_q. The molar cation polarizability values of Te^{4+} (α_{Te}=1.595 Å^3), Se^{6+} (α_{Se} = 0.075 Å^3) and Na^+ (α_{Na} = 0.181 Å^3) ions[63]. The calculated values of $\alpha_o^{2-}(E_{opt})$ are listed in Table 7. It is noticed from the Table 7 that $\alpha_o^{2-}(E_{opt})$values increases from 2.911-3.469 as Na_2O content increases from 5 to 20 mol % in the glass samples. The values of the optical energy band gap based oxide ion polarizability have an increasing trend. The increasing trend due to increasing amount of non-bridging oxygens that has high polarizability as the concentration of sodium oxide increases in the glass system. The increase in non-bridging oxygen number can be confirmed in the FTIR result where the fractions of TeO_3 structural units with non-bridging

oxygen increases while the fraction of TeO_4 structural units with bridging oxygens decreases. The values of α_o^{2-}, R_M, and α_m have shown increasing trend with increasing Na_2O content in the present glass samples. The increase in refractive index is a result of the decrease in optical band gap values. At the same time, molar refraction increased with an increase in refractive index, which in turn increased both oxide ion polarizability and molar polarizability of the glass samples.

The optical basicity 'Λ' on the basis of E_{opt} and 'n' are calculated[64] using the following relation:

$$\Lambda = 1.67\left(1 - \frac{1}{\alpha_o^{2-}}\right) \quad \ldots (18)$$

The obtained values of optical basicity of E_{opt} values are listed in Table 7. The values of optical basicity of E_{opt} lie between 1.096 and 1.188 in the present glass system. The $\Lambda(E_{opt})$ values are increasing as Na_2O content increases from 5 to 20 mol % in the glass samples. The optical basicity is associated with the electron power of the oxygen in glasses. The low value of optical basicity refers to a covalent bonding and high value refers to more ionic bonding. So, it helps in the assessment of the type of bonds present in the tested glass sample. By using this relation, the increase in the oxide ion polarizability increases the optical basicity, it results in an increase in the refractive index and decrease in the optical band gap. The increase in the optical basicity suggests that the cation-oxygen bonds are becoming more ionic than covalent. The increase in the optical basicity also suggests that the number of non-bridging oxygens (NBOs) are created than bridging oxygens (BOs). The similar behavior observed by N. Elkhoshkhany et al. in the TeO_2–ZnO–Nb_2O_5–Gd_2O_3glass system[56].

According to ultra-violet absorption bands, the extinction coefficient (k) obeys Fermi-Dirac distribution function[61, 65] for the different glass samples.

$$k(\lambda) = \frac{1}{1+exp[E-E_F/k_B T]} \quad \ldots (19)$$

Where, $E = hc/\lambda$ is the variable photon energy to investigate the sample, 'h' is planks constant, 'c' is the velocity of light in free space, 'E_F' is the Fermi energy, k_BT is the thermal energy due to absolute temperature $T=297$ K, 'k_B' is the Boltzmann constant. By linear fitting of the Eq. (19), the Fermi energy values are evaluated for the present glass system and are listed in Table 7. The obtained high Fermi energy values are ($\gg k_BT$) reliable with the property that tested glass samples are of dielectric nature.

The optical response of a glass sample is mainly studied in terms of the optical conductivity (σ) which is given by the relation[66]:

$$\sigma = \frac{\alpha nc}{4\pi} \quad \ldots (20)$$

Where, 'α' is the absorption coefficient, 'c' is the velocity of light and 'n' is the refractive index.

The Fig. 14 shows the variation of optical conductivity (σ) vs photon energy for the tested glass samples. It is seen clearly that the optical conductivity directly depends on the refractive index and absorption coefficient of the glass sample. It follows the same trend as that of the absorption coefficient and refractive index with an increase of wavelength. It is observed from the Fig. 14 that the optical conductivity increases with photon energy for all the glass samples. The increase in optical conductivity can be assigned to increase in absorption coefficient.The maximum value of the optical conductivity for the glass samples IITSN2, IITSN3, IITSN4 and IITSN5 are 1.83 x 10^{11} ohm^{-1}-m^{-1}, 2.789 x 10^{11} ohm^{-1}-m^{-1} , 2.375 x 10^{11} ohm^{-1}-m^{-1} and 2.950 x 10^{11} ohm^{-1}-m^{-1} at 4.5 eV, respectively.

The single-effective oscillator model was proposed by Wemple and Di Domenico[67]. Using this model the single- oscillator parameters (E_d, E_0) are calculated and listed in the Table 7. This model describes an important role in determining the behavior of the refractive index. The optical data of the refractive index can be described by the single-oscillator model is:

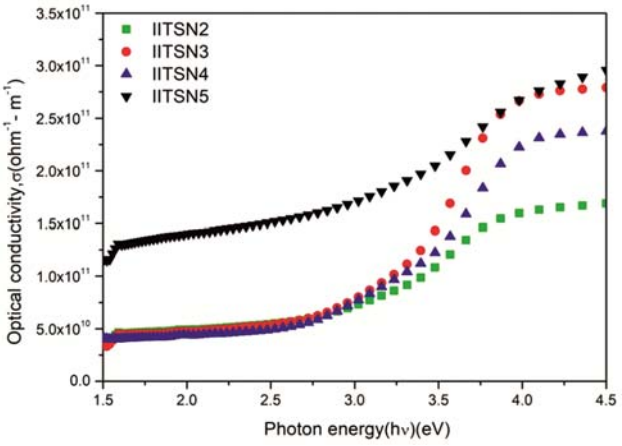

Fig. 14 – Variation of optical conductivity as a function of photon energy for 80 TeO_2-(20-x) SeO_2-xNa_2O (where x=5, 10, 15, 20 mol %) glass system.

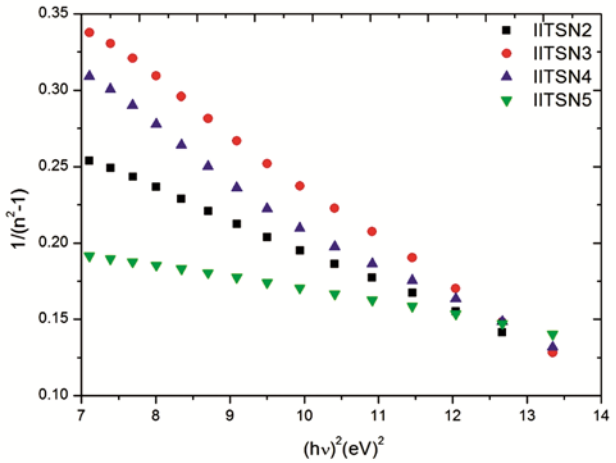

Fig. 15 – The variation of *1/ (n^2-1)* and E^2 for the present glass system for 80 TeO_2-(20-x) SeO_2-xNa_2O (where x=5, 10, 15, 20 mol %) glass system.

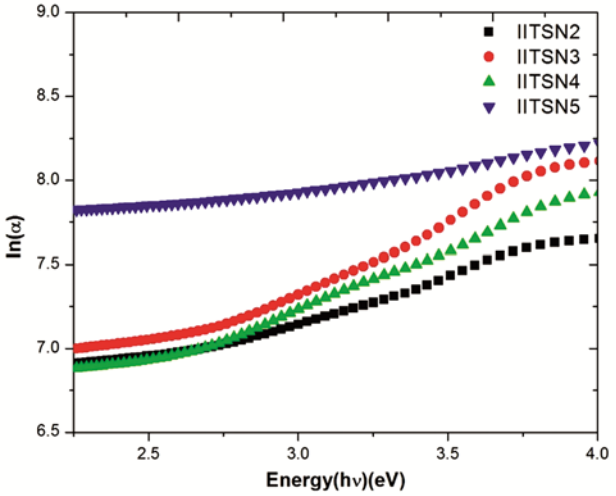

Fig. 16 – Urbach plot of 80TeO_2-(20-x) SeO_2-xNa_2O (where x=5, 10, 15, 20 mol %) glass system.

$$n^2 - 1 = \frac{E_d E_0}{E_0^2 - (h\nu)^2} \quad \ldots (21)$$

Where, '*hv*' is the photon energy, '*n*' is the refractive index, 'E_d' is the dispersion energy, measures the average strength of the inter band optical transitions and 'E_0' is the single oscillator energy and also called the average excitation energy for an electronic transition. The Fig. 15 shows the variation of *1/ (n^2-1) vs.* E^2. The plotting *1/ (n^2-1) vs* E^2 allow us to evaluate the single-oscillator parameters by linear fitting to the points in the Fig. 15. E_d and E_0 can be evaluated from the slope $(E_0E_d)^{-1}$ and intercept (E_0/E_d) on the vertical axis. The obtained values of E_d and E_0 are listed in Table 7. The low E_d values are observed indicates strong iconicity exists in the glass samples[67].

The Urbach plot has been shown in Fig. 16. Urbach energy ΔE is evaluated by taking the reciprocals of the slopes of the linear portion of the *ln(α) vs hv* curves. The obtained values of Urbach energy are listed in Table 7. The value of Urbach energy increases as Na_2O mol % increases. The increase in Urbach energy indicates that the degree of disorder increases in the glass matrix[56] and also increases the number of defects in the glass system[50].

4 Conclusions

TeO_2-SeO_2-Na_2O glass systems have been prepared by using melting and quenching technique. From the physical properties, it has been observed that formation of less dense structure and less tightly packing results in degradation of the structural units and formation of non-bridging oxygen sites in the glass matrix. The structural investigation of TeO_2-SeO_2-Na_2O glass system reveals the formation of Se-O^-, Se=O, TeO_{3+1}, TeO_3 units in the glass structure. The results suggest that increasing the Na_2O content acts as a network modifier by breaking of the network structure while decreasing the SeO_2 content acts as a network former in the structure. E_{opt} values obtained from absorption spectra, imaginary part of dielectric constant measurements are in good agreement with the exponent *n=1/2*. So, direct band exists in the glass system. The optical band gap values are found to decrease with increase in Na_2O content. The optical band gap energy values suggest that NBOs concentration increases as Na_2O content increases in the glass samples, which lowers the band gap energy.The theory of metallization criterion revels the present glass system's non-metallic or insulating nature. The values of α_o^{2-}, R_M, and α_m have shown increasing trend with increasing Na_2O content in the glass sample. The optical basicity value increases as Na_2O mol % increases in the present glass system. From the obtained high Fermi energy values ($\gg k_BT$) that the tested glass samples are in dielectric nature. The increase in optical conductivity can be assigned to increase in absorption coefficient. The low E_d values indicate iconicity exists in the glass samples. As Na_2O content increases in the glass system the Urbach energy increases that lead to an increase in the degree of disorder in the glass matrix.

References

1 Kavaklıoglu K B, Clikbilek M C, Ersundu A E & Aydin S, *Materials Science and Technology conference and Exhibition Proceedings*, Edt by Du J & Kieffer J, Pittsburgh, PA, 1 (2012) 237.

2 Celikbilek M, Ersundu A E, Solak N & Aydin S, *J Alloys Compd*, 509 (2011) 5646.
3 Ersundu A E, Karaduman G, Celikbilek M, Solak N & Aydin S, *J Eur Ceram Soc*, 30 (2010) 3087.
4 Ersundu A E, Celikbilek M, Solak N & Aydin S, *J Eur Ceram Soc*, 31 (2011) 2775.
5 Yardımcı D, Celikbilek M, Ersundu A E & Aydin S, *Mater Chem Phys*, 137 (2013) 999.
6 Ersundu A E, Karaduman G, Celikbilek M, Solak N & Aydin S, *J Alloys Compd*, 508 (2010) 266.
7 Karaduman G, Ersundu A E, Celikbilek M, Solak N & S Aydin, *J Eur Ceram Soc*, 32 (2012) 603.
8 Celikbilek M, Ersundu A E, Solak N & Aydin S, *J Non-Cryst Solids*, 357 (2011) 88.
9 Ersundu A E, Celikbilek M & Aydin S, *J Non-Cryst Solids*, 358 (2012) 641.
10 El-Mallawany R A H, Tellurite Glasses Handbook CRC Press, Boca Raton, 2002.
11 Bachvarova-Nedelcheva A, Iordanova R, Yordanov S & Dimitriev Y, *J Non-Cryst Solids,* 355 (2009) 2027.
12 Govindaraj G, Baskaran N, Shahi K & Monoravi P, *Solid State Ionics*, 76 (1995) 47.
13 Machida N, Chusho M & Minami T, *J Non-Cryst Solids*, 101 (1988) 70.
14 Pal M, Hirota K, Tsujigami Y & Sakata H, *J Phys D: Appl Phys*, 34 (2001) 459.
15 Chowdari B V R & Kumar P P, *Solid State Ionics*, 113 (1998) 665.
16 Sunandana C & Bhatnagar A, *J Phys*, C17 (1984) 467.
17 Abe M, Benino Y, Fujiwara T & Komatsu T, *J Appl Phys*, 97 (2005) 123516.
18 Dimitriev Y, Ivanova Y & Dimitrov V, *J Mater Sci Lett*, 9 *(1990)* 793.
19 Dimitriev Y, Yordanov S & Lakov L, *J Non-Cryst Solids*, 293 (2001) 410.
20 Lakshminarayana G, Kaky K M, Baki S O, Lira A N, P, Kityk I V & Mahdi M A, *J Alloys Compd,* 690 (2017) 799.
21 Halimah M K, Daud W M, Sidek H A A, Zaidan A W & Zainal A S, *Mater Sci-Poland*, 28 (2010) 173.
22 Ahmmad S, Samee M A, Edukondalu A & Rahman S, *Res Phys,* 2 (2012) 175.
23 Samdani, Shareefuddin M, Ramadevudu G, S Laxmi S R & Narasimha M C, *ISRN Ceramics*, 2013 (2013) 419183.
24 Celikbilek Miray, Ersundu A E & Aydin S, *J Am Ceram Soc,* 96 (2013) 1470.
25 Kutlu B, Kavakloglu, Aydin S, Çelikbilek M & Ersundu A E, *Int J Appl Glass Sci*, 6(4) (2015) 406.
26 Bachvarova-Nedelcheva A, Iordanova R, Kostov K L, Yordanov S & Ganev V, *Opt Mater*, 34 (2012) 1781.
27 Salehizadeh S A, Melo B M G, Freire F N A, Valente M A & Graça M P F, *J Non-Cryst Solids*, 443 (2016) 65.
28 Pascuta P, Pop L, Rada S, Bosca M & Culea E, *J Mater Sci: Mater Electron*, 19 (2008) 424.
29 Zayas M E, Arizpe H, Castillo S J, Medrano F, Diaz G C, Rincon J M & Romero M, *Phys Chem Glasses*, 46 (2005) 46.
30 Jimenez–Sandoval S, Lopez–Lopez S, Chao B S & Melendez–Lira M, *Thin solid films*, 342 (1999) 1.
31 Ruvalcaba-Cornejo C, Zayas Mae, Castillo S J, Lozada-Morales R, Perez-Tello M, Díaz C G & Rincon J M, *Optic Mater*, 33 (2011) 823.
32 Chowdari V R & Kumari P, *Mater Res Bull,* 34 (1999) 327.
33 Li H, Su Y & Sundaram S K, *J Non-Cryst Solids,* 293 (2001) 402.
34 Duveger C, Bouazaoui M & Turrel S, *J Non-Cryst Solids,* 220 (1997) 169.
35 Suresh S, Pavani P G & Mouli V C, *Mat Res Bull,* 47 (2012) 724.
36 Sekiya T, Mochida N & Kurita S, *J Cer Soc Jpn,* 108 (2000) 236.
37 Upender G, Vardhani C P, Suresh S, Awasthi A M & Mouli V C, *Mat Chem Phys,* 121 (2010) 335.
38 Tatssumisago M, Kato S I, Minami T & Kowada Y, *J Non-Cryst Solids,* 192 (1994) 478.
39 Tatsumisago M, Minami T, Kowada Y & Adachi H, *Phys Chem Glass,* 35 (1994) 89.
40 Heo J, Lam D, Sigel G H, Mendoza E A & Hensley D A *J Am Ceram Soc*, 75 (1992) 277.
41 Komatsu T, Tawarayama H, Mohri H & Matusita K, *J Non-Cryst Solids,* 135 (1991) 105.
42 Hager I Z & El-Mallawany R, *J Mater Sci,* 45 (2010) 897.
43 Sekiya T, Mochida N, Ohtsuka A & Tonokawa M, *J Non-Cryst Solids,*144 (1992) 128.
44 Lefterova E D & Angelov P V, *Phys Chem Glass,* 41 (2000) 192.
45 Bachvarova A, Dimitriev Y & Iordanova R, *J Non-Cryst Solids,* 351 (2005) 998.
46 Bachvarova-Nedelcheva A, Iordanova R, Kostov K L, Ganev V & Yordanov S, *Opt Mater,* 36 (2014) 1319.
47 Ahmad S K, Samee M A, Taqiullah S M & Rahman S, *J Taibah Univ Sci,* 10 (2016) 329.
48 Rada S, Culea E, Rus V, Pica M & Culea M, *J Mater Sci,* 43 (2008) 3713.
49 Rada S, Culea M & Culea E, *J Non- Cryst Solids*, 354 (2008) 5491.
50 Palui A & Ghosh A, *J Phys Chem C*, 121 (2017) 8738.
51 Dimitriev Y, Ivanova I & Dimitrov V, *J Mater Sci,* 21 (1986) 142.
52 Urbach F, *Phys Rev,* 92 (1953) 1324.
53 Tauc J & Menth A, *J Non-Cryst Solids*, 8 (1972) 569.
54 Gosain D P, Shimizu T, Ohmura M, Suzuki M, Bando T & Okano S, *J Mater Sci,* 26 (1991) 2371.
55 Escobar-Alarcon L, Arrieta A, Camps E, Muhl S, Rodil S & Vigueras-Santiago E, *Appl Sur Sci,* 254 (2007) 412.
56 Elkhoshkhany N, Abbas Rafik, El-Mallawany R & Fraih A J, *Ceram Int*, 40 (2014) 14477.
57 Sushama D & Predeep P, *Int J Appl Phys Math,* 4 (2014)139.
58 El-Mallawany R, Abdalh M D & Ahmed I A, *Mater Chem Phys*, 109 (2008) 291.
59 Dimitrov V & Sakka S, *J Appl Phys*, 79 (1996)1736.
60 Herzfeld K, *Phys Rev*, 29(1927) 701.
61 El-Diasty F, Wahab F A A & Abdel-Baki M, *J Appl Phys*, 100 (2006) 093511.
62 Halimah M K, Faznny M F, Azlan M N & Sidek H A A, *Res Phys*, 7 (2017) 581.
63 Dimitrov V & Sakka S, *J Appl Phys,* 79 (1996)1736.
64 Dimitrov V & Komatsu T, *J Univ Chem Tech Metal,* 45 (2010) 219.
65 Jiles, Introduction to the Electronic Properties of Materials, 1st Edn (Chapman and Hall, London), 1994
66 Sharma P & Katyal S C, *J Phys D: Appl Phys*, 40 (2007) 2115.
67 Wemple S H, Domenico D M,*Phys Rev B*, 3 (1971) 1338.
68 Zachariasen W H, *J Am Chem Soc*, 54 (1932) 3841.